

Chapter 2

Relation Between Confinement and Chiral Symmetry Breaking

Abstract In this chapter, we discuss the relation between confinement and chiral symmetry breaking in QCD using some analytical formulae connecting order parameters for confinement and the Dirac eigenmodes in the lattice QCD. We consider the Polyakov loop, its fluctuations, and the Wilson loop as the order parameters for quark-confinement. The analytical formulae indicate no direct one-to-one correspondence between confinement and chiral symmetry breaking in QCD.

Keywords Dirac eigenmodes · Polyakov loop and its fluctuations · Wilson loop · Elitzur's theorem · Temporally odd-number lattice

2.1 Polyakov Loop

In this section, we discuss the relation between confinement and chiral symmetry breaking in QCD by deriving several analytical formulae connecting the Polyakov loop and the Dirac eigenmodes.

2.1.1 Operator Formalism and Dirac Modes on Lattice

In order to derive the relations, we first prepare the operator formalism and the Dirac modes in the $SU(N_c)$ lattice QCD [1, 2].

The link-variable operator $\hat{U}_{\pm\mu}$ is defined as the matrix element

$$\langle s | \hat{U}_{\pm\mu} | s' \rangle = U_{\pm\mu}(s) \delta_{s \pm \hat{\mu}, s'}, \quad (2.1)$$

where s denotes the site on the lattice and $\hat{\mu}$ is the unit vector in direction μ in the lattice unit. Using the link-variable operator, the several quantity can be redefined. The covariant derivative operator \hat{D}_μ on the lattice expressed as

$$\hat{D}_\mu = \frac{1}{2a}(\hat{U}_\mu - \hat{U}_{-\mu}) \quad (2.2)$$

corresponding to the matrix element (3.2). And then the naive Dirac operator on the lattice $\hat{\mathcal{D}}$ can be given by

$$\hat{\mathcal{D}} = \gamma_\mu \hat{D}_\mu = \frac{1}{2a} \sum_{\mu=1}^4 \gamma_\mu (\hat{U}_\mu - \hat{U}_{-\mu}). \quad (2.3)$$

Corresponding to Eqs. (1.12), (1.13), and (1.14), the eigenvalue equation of the naive Dirac operator is

$$\hat{\mathcal{D}}|n\rangle = i\lambda_n|n\rangle \quad (2.4)$$

with the completeness relation the chiral symmetry

$$\langle m|n\rangle = \delta_{mn} \quad (2.5)$$

$$\{\mathcal{D}, \gamma_5\} = 0. \quad (2.6)$$

The coordinate representation of the eigenstate is expressed as the eigenfunction $\psi_n(s) \equiv \langle s|n\rangle$, and the explicit form for the Dirac eigenvalue equation is written by

$$\frac{1}{2a} \sum_{\mu=1}^4 \gamma_\mu [U_\mu(s)\psi_n(s + \hat{\mu}) - U_{-\mu}(s)\psi_n(s - \hat{\mu})] = i\lambda_n\psi_n(s). \quad (2.7)$$

Here, the link-variables are given by the Monte-Carlo simulation in the lattice QCD, and then the eigenfunction can be directly calculated. The Dirac eigenfunction $\psi_n(s)$ has an irrelevant phase factor $e^{i\varphi_n[V]}$ because $\psi_n(s)$ is gauge-transformed as

$$\psi_n(s) \rightarrow V(s)\psi_n(s), \quad (2.8)$$

by the gauge transformation of $U_\mu(s) \rightarrow V(s)U_\mu(s)V^\dagger(s + \hat{\mu})$. The transformation law is the same as that of the quark field. This mode-dependent global phase factor corresponds to arbitrariness of the phase in the basis $|n\rangle$ [1].

The antiperiodic boundary condition for the imaginary-time direction is necessary for the finite-temperature formalism. Thus, we impose the antiperiodic boundary condition to the link-variable operator as

$$\begin{aligned} \langle \mathbf{s}, N_\tau | \hat{U}_4 | \mathbf{s}, 1 \rangle &= -U_4(\mathbf{s}, N_\tau), \\ \langle \mathbf{s}, 1 | \hat{U}_{-4} | \mathbf{s}, N_\tau \rangle &= -U_{-4}(\mathbf{s}, 1) = -U_4^\dagger(\mathbf{s}, N_\tau). \end{aligned} \quad (2.9)$$

at the temporal boundary $t = N_\tau (= 0)$ [3]. This temporal boundary condition does not influence the plaquette action and the clover term because they are constituted

of the spatial loop of the link-variables. If a loop crosses the temporal boundary, the minus sign appear twice and they are canceled in the loop.

Next, the Polyakov loop, which is an order parameter for the quark-confinement, is expressed as

$$L = -\frac{1}{N_c V} \text{Tr}_c \{ \hat{U}_4^{N_\tau} \} = \frac{1}{N_c V} \sum_s \text{tr}_c \left\{ \prod_{n=0}^{N_\tau-1} U_4(s + n\hat{4}) \right\}, \quad (2.10)$$

using the link-variable operators, where Tr_c is the functional trace, $\text{Tr}_c \equiv \sum_s \text{tr}_c$, taken over the indices of sites and colors. The minus sign in the definition comes from the additional minus on $U_4(s, N_\tau)$ in Eq. (2.9).

We discuss the property of the Dirac-mode matrix element of the link-variable operator $\langle m | \hat{U}_\mu | n \rangle$. It can be explicitly written as

$$\begin{aligned} \langle m | \hat{U}_\mu | n \rangle &= \sum_s \langle m | s \rangle \langle s | \hat{U}_\mu | s + \hat{\mu} \rangle \langle s + \hat{\mu} | n \rangle \\ &= \sum_s \psi_m^\dagger(s) U_\mu(s) \psi_n(s + \hat{\mu}). \end{aligned} \quad (2.11)$$

This quantity is gauge invariant for the arbitrary modes $|n\rangle$, and $|m\rangle$. In fact, by the gauge transformation Eq. (2.8), the matrix element is transformed as

$$\begin{aligned} \langle m | \hat{U}_\mu | n \rangle &= \sum_s \psi_m^\dagger(s) U_\mu(s) \psi_n(s + \hat{\mu}) \\ &\rightarrow \sum_s \psi_m^\dagger(s) V^\dagger(s) \cdot V(s) U_\mu(s) V^\dagger(s + \hat{\mu}) V(s + \hat{\mu}) \psi_n(s + \hat{\mu}) \\ &= \sum_s \psi_m^\dagger(s) U_\mu(s) \psi_n(s + \hat{\mu}) = \langle m | \hat{U}_\mu | n \rangle. \end{aligned} \quad (2.12)$$

However, the irrelevant n -dependent phase factor appears. Nevertheless, this phase factor cancels as $e^{i\varphi_n[V]} e^{-i\varphi_n[V]} = 1$ in the diagonal element $|n\rangle$ and $\langle n|$. In fact, physical quantities such as the Wilson loop and the Polyakov loop have only the diagonal element [1–3].

2.1.2 The Relation Between Polyakov Loop and Dirac Modes on the Temporally Odd-Number Lattice

Then, we analytically derive the relations connecting the Polyakov loop and the Dirac modes. First, we derive the analytical relation for the naive Dirac operator (2.3) on the on the temporally odd-number lattice, where the temporal lattice size is odd number. Then, the relation will be generalized for the even lattice.

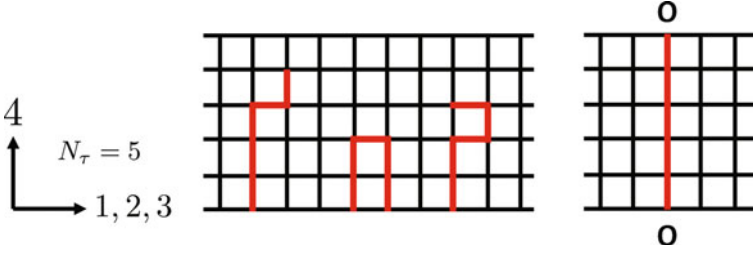


Fig. 2.1 An example of odd lattice. This is $N_\tau = 5$ case. Each line corresponds to each term in $\hat{U}_4 \hat{\mathcal{P}}^{N_\tau-1}$ in Eq.(2.14). All the lines in the *left figure* correspond to the gauge-variant terms while the line in the *right figure* is the unique closed loop using the temporal periodicity, namely the Polyakov loop

First of all, consider products of the link-variable operators which correspond to each path. If the path is a closed loop, the functional trace of the associated products of the link-variable operator is gauge invariant and an observable. However, if the path is not a closed loop, the corresponding quantity is gauge variant and exactly zero as

$$\begin{aligned}
 \text{Tr}_c(\hat{U}_{\mu_1} \hat{U}_{\mu_2} \cdots \hat{U}_{\mu_N}) &= \text{tr}_c \sum_s \langle s | \hat{U}_{\mu_1} \hat{U}_{\mu_2} \cdots \hat{U}_{\mu_N} | s \rangle \\
 &= \text{tr}_c \sum_s U_{\mu_1}(s) U_{\mu_2}(s + \hat{\mu}_1) \cdots U_{\mu_N} \left(s + \sum_{k=1}^{N-1} \hat{\mu}_k \right) \left\langle s + \sum_{k=1}^N \hat{\mu}_k | s \right\rangle \\
 &= 0,
 \end{aligned} \tag{2.13}$$

where $\sum_{k=1}^N \hat{\mu}_k \neq 0$ is satisfied for non-closed path and N is the length of the path. This is due to the definition of the link-variable operator Eq.(2.1). Also, this fact is understood from Elitzur's theorem [4] that the vacuum expectation values of gauge-variant operators are zero.

We consider the temporally odd number lattice shown in Fig.2.1 because the later discussion is very simple and understandable. We use the spatially symmetric lattice, i.e., $N_1 = N_2 = N_3 \equiv N_\sigma$ and $N_4 \equiv N_\tau$, and assume that the spatial length is larger than temporal length. The periodic boundary conditions are imposed on both temporal and spatial directions. These assumptions are not unnatural because the temporal length is finite and the spatial length is infinite in the ideal situation for the continuum theory at finite temperature.

On such a lattice, we introduce a functional trace I defined as

$$I = \text{Tr}_{c,\gamma}(\hat{U}_4 \hat{\mathcal{P}}^{N_\tau-1}). \tag{2.14}$$

Substituting the definition of the Dirac operator (2.3), the functional trace I is expressed as a sum of products of odd-number link-variable operators because N_τ

is odd number. Some examples are shown in Fig. 2.1. Note that most of the terms in the expansion of I exactly vanish because one cannot make a closed loop by using odd-number link-variable operators on a square lattice. Thus there is only contribution from the closed path due to the temporal periodicity, that is the Polyakov loop L , which can be closed loop and gauge invariant with odd-number link-variables using the periodic boundary condition. This is why we use the temporally odd-number lattice. In this way, the functional trace I can be expressed as

$$\begin{aligned}
 I &= \text{Tr}_{c,\gamma}(\hat{U}_4 \hat{\mathcal{D}}^{N_\tau-1}) \\
 &= \text{Tr}_{c,\gamma}\{\hat{U}_4(\gamma_4 \hat{D}_4)^{N_\tau-1}\} \\
 &= 4\text{Tr}_c(\hat{U}_4 \hat{D}_4^{N_\tau-1}) \\
 &= \frac{4}{(2a)^{N_\tau-1}} \text{Tr}_c\{\hat{U}_4(\hat{U}_4 - \hat{U}_{-4})^{N_\tau-1}\} \\
 &= \frac{4}{(2a)^{N_\tau-1}} \text{Tr}_c\{\hat{U}_4^{N_\tau}\} \\
 &= -\frac{12V}{(2a)^{N_\tau-1}} L.
 \end{aligned} \tag{2.15}$$

On the other hand, using the completeness of the Dirac mode, the functional trace is expressed as

$$I = \sum_n \langle n | \hat{U}_4 \hat{\mathcal{D}}^{N_\tau-1} | n \rangle = i^{N_\tau-1} \sum_n \lambda_n^{N_\tau-1} \langle n | \hat{U}_4 | n \rangle. \tag{2.16}$$

Therefore, combining Eqs. (2.15) and (2.16), we find a relation

$$L = -\frac{(2ai)^{N_\tau-1}}{12V} \sum_n \lambda_n^{N_\tau-1} \langle n | \hat{U}_4 | n \rangle. \tag{2.17}$$

This is a relation directly connecting the Polyakov loop and the Dirac modes, i.e., a Dirac spectral representation of the Polyakov loop.

Note that Eq. (2.17) is gauge invariant relation because the Polyakov loop is gauge invariant quantity and the Dirac modes can be gauge-covariantly calculated. Thus our discussion perfectly respects the gauge symmetry. The relation holds for each gauge configuration, namely an arbitrary set of the link-variables. Consequently, this relation is satisfied regardless of whether the gauge-configuration is generated in full QCD or quenched QCD. However, the Dirac modes, λ_n and $|n\rangle$, are calculated by use of the naive Dirac operator (2.3). This point is generalized in the later section. Of course, the configuration average of the formula (2.17) is valid.

$$\langle L \rangle = -\frac{(2ai)^{N_\tau-1}}{12V} \left\langle \sum_n \lambda_n^{N_\tau-1} \langle n | \hat{U}_4 | n \rangle \right\rangle. \tag{2.18}$$

The outmost bracket $\langle \rangle$ means gauge-configuration average.

From the analytical relation (2.17), the relation between confinement and chiral symmetry breaking in QCD because the Polyakov loop is an order parameter for quark-confinement and the Dirac modes are strongly related with the chiral symmetry breaking via the Banks–Casher relation (1.26). First, we note that the Dirac matrix element is finite: $|\langle n | \hat{U}_4 | n \rangle| < 1$. Thus, we can find that the factor $\lambda_n^{N_\tau-1}$ determines the magnitude of the contribution from each Dirac mode $\lambda_n^{N_\tau-1} \langle n | \hat{U}_4 | n \rangle$. The overall factor is not related with the comparison of the magnitude of each contribution. However, when the Dirac eigenvalue is small $|\lambda_n| \simeq 0$, the factor $\lambda_n^{N_\tau-1}$ plays as the damping factor. Thus, the contributions from the low-lying Dirac modes are strongly suppressed compared to the other Dirac-mode contribution. However, as discussed in the previous sections, the low-lying Dirac modes are essential modes for the chiral symmetry breaking. Thus, the negligible contribution from the low-lying Dirac modes to the Polyakov loop indicates that the important modes for the chiral symmetry breaking are not important for quark-confinement in QCD. In other words, our analytical discussion suggests that there are no direct one-to-one correspondence between quark-confinement and chiral symmetry breaking in QCD.

In order to derive the relation (2.17), we assume only the following conditions:

1. odd N_τ
2. square lattice
3. temporal periodicity for link-variables

Due to the first assumption, the analytical relation (2.17) is satisfied only on the temporally odd-number lattice. However, this constraint is not so serious because this choice of the parity for the lattice size does not alter the physics in the continuum limit with any large number of N_τ . In fact, the relation (2.17) can be generalized for the even lattice with even N_τ . By the same reason, the second assumption is also not problem. The third assumption is necessary for the finite-temperature formalism. Therefore, the relation (2.17) is fully general and valid in full QCD and in finite temperature and density, and furthermore regardless of the phase of the system. In other words, the relation holds in confinement and deconfinement phases, and in chiral broken and restored phases.

One might consider that the Polyakov loop and the Dirac modes are not related each other because the Polyakov loop is defined by gauge fields alone and the Dirac modes look are fermionic modes. However, the Polyakov loop is influenced by the quarks, and the Dirac modes are strongly affected by the gauge fields because the Dirac eigenvalue equation (2.7) includes the link-variables. A similar example is instantons. The instantons are defined by gauge fields alone, however they have a close connection to the axial U(1) anomaly, which relates to a fermionic symmetry. Thus, it is not unnatural that the Polyakov loop has a connection to the Dirac modes. Thus, when the dynamical quarks are considered, its effect changes the values of the Polyakov loop L , the Dirac eigenvalue distribution $\rho(\lambda)$ and the matrix elements $\langle n | \hat{U}_\mu | m \rangle$. However, the relation Eq.(2.17) holds even if considering the dynamical quarks.

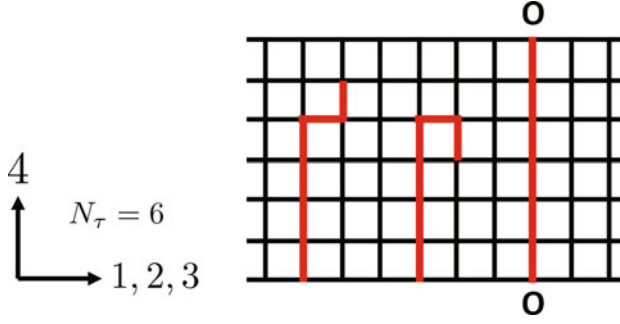


Fig. 2.2 An example of even lattice. This is $N_\tau = 6$ case. Each line corresponds to each term in $\hat{U}_4^{N_\tau/2+1} \hat{\mathcal{P}}^{N_\tau/2-1}$ in Eq. (2.19). The Polyakov loop is the unique closed loop using the temporal periodicity

2.1.3 The Relation Between Polyakov Loop and Dirac Modes on the Even Lattice

Moreover, the Polyakov loop can be expressed in terms of the Dirac modes on the even lattice where all the lattice sizes are even number with the periodic boundary condition for link-variables [2]. It is also derived in the following.

Corresponding to I in Eq. (2.14), we introduce a quantity

$$\tilde{I}(N_\tau) \equiv \text{Tr}_{c,\gamma}(\gamma_4^{\xi(N_\tau)} \hat{U}_4^{N_\tau/2+1} \hat{\mathcal{P}}^{N_\tau/2-1}) \quad (2.19)$$

with $\xi(N_\tau)$ is defined as

$$\xi(N_\tau) = \begin{cases} 0 & (N_\tau/2 : \text{odd}) \\ 1 & (N_\tau/2 : \text{even}) \end{cases} \quad (2.20)$$

This quantity $\hat{U}_4^{N_\tau/2+1} \hat{\mathcal{P}}^{N_\tau/2-1}$ can be expanded as a sum of products of N_τ link-variable operators. An example for the even lattice is shown in Fig. 2.2 and each line corresponds with each term in the expansion of $\hat{U}_4^{N_\tau/2+1} \hat{\mathcal{P}}^{N_\tau/2-1}$ in Eq. (2.19). In $\hat{U}_4^{N_\tau/2+1} \hat{\mathcal{P}}^{N_\tau/2-1}$, any spatially closed loops cannot be made because the number of \hat{U}_4 is larger than that of \hat{U}_{-4} . Then, $\hat{U}_4^{N_\tau/2+1} \hat{\mathcal{P}}^{N_\tau/2-1}$ does not have any gauge-invariant quantities except for the Polyakov loop, which is the temporally closed loop. Therefore using the temporal periodic boundary condition, one finds

$$\begin{aligned}
\tilde{I} &= \text{Tr}_{c,\gamma}(\gamma_4^{\xi(N_\tau)} \hat{U}_4^{N_\tau/2+1} \hat{p}^{N_\tau/2-1}) \\
&= \text{Tr}_{c,\gamma}\{\gamma_4^{\xi(N_\tau)} \hat{U}_4^{N_\tau/2+1} (\gamma_4 \hat{D}_4)^{N_\tau/2-1}\} \\
&= \text{Tr}_{c,\gamma}(\gamma_4^{\xi(N_\tau)+N_\tau/2-1} \hat{U}_4^{N_\tau/2+1} \hat{D}_4^{N_\tau/2-1}) \\
&= 4\text{Tr}_c(\hat{U}_4^{N_\tau/2+1} \hat{D}_4^{N_\tau/2-1}) \\
&= \frac{4}{(2a)^{N_\tau/2-1}} \text{Tr}_c\{\hat{U}_4^{N_\tau/2+1} (\hat{U}_4 - \hat{U}_{-4})^{N_\tau/2-1}\} \\
&= \frac{4}{(2a)^{N_\tau/2-1}} \text{Tr}_c\{\hat{U}_4^{N_\tau}\} \\
&= \frac{12V}{(2a)^{N_\tau/2-1}} L.
\end{aligned} \tag{2.21}$$

On the other hand, taking Dirac modes as the basis for the functional trace in Eq. (2.19), the quantity \tilde{I} is expressed as

$$\begin{aligned}
\tilde{I} &= \sum_n \langle n | \gamma_4^{\xi(N_\tau)} \hat{U}_4^{N_\tau/2+1} \hat{p}^{N_\tau/2-1} | n \rangle \\
&= i^{N_\tau/2-1} \sum_n \lambda_n^{N_\tau/2-1} \langle n | \gamma_4^{\xi(N_\tau)} \hat{U}_4^{N_\tau/2+1} | n \rangle.
\end{aligned} \tag{2.22}$$

Combining Eqs. (2.21) and (2.22), the relation is found as

$$L = \frac{(2ai)^{N_\tau/2-1}}{12V} \sum_n \lambda_n^{N_\tau/2-1} \langle n | \gamma_4^{\xi(N_\tau)} \hat{U}_4^{N_\tau/2+1} | n \rangle. \tag{2.23}$$

In this way, we derive the relation connecting the Polyakov loop L and the Dirac eigenvalues $i\lambda_n$ on the even lattice. Comparing Eqs. (2.17) and (2.23), the form of Eq. (2.17) is simpler than that of Eq. (2.23). However, both equations give the same content of physics because it should be independent of the temporal lattice size N_τ . The dumping factor $\lambda_n^{N_\tau/2-1}$ in RHS of Eq. (2.23) and $\lambda_n^{N_\tau-1}$ in RHS of Eq. (2.17) are expected to have the same roles.

As we discuss in the previous section, the analytical relations Eqs. (2.17) and (2.23) indicate small contribution from low-lying Dirac modes to the Polyakov loop. However, it is also important to quantitatively confirm the expectation. For simplicity, we consider the temporally odd-number lattice, namely Eq. (2.17).

Since Eq. (2.17) is given as a sum over all the Dirac modes, each term expresses the individual contribution from each Dirac mode and it can be numerically obtained for the quantitative discussion. In the relation (2.17), the Dirac matrix element $\langle n | \hat{U}_\mu | m \rangle$ can be explicitly written as Eq. (2.11). Thus, the relation (2.17) is expressed as

$$L = -\frac{(2ai)^{N_\tau-1}}{12V} \sum_n \lambda_n^{N_\tau-1} \sum_s \psi_n^\dagger(s) U_4(s) \psi_n(s + \hat{4}). \tag{2.24}$$

In principle, the Dirac eigenvalues λ_n and the Dirac eigenfunctions $\psi_n(s)$ in RHS of Eq. (2.24) can be obtained by solving the Dirac eigenequation (2.7) for each gauge configuration generated in the Monte-Carlo simulation. However, it is not easy task because the numerical cost for solving the Dirac eigenequation is very large. In fact, the dimension of the Dirac operator $(4 \times N_c \times V)^2$, it is very huge in general. Nevertheless, using the Kogut–Susskind (KS) formalism [5], the numerical cost can be partially reduced without approximation. We discuss it in the next part.

2.1.4 Modified Kogut–Susskind Formalism for Temporally Odd-Number Lattice

All the eigenvalues and the eigenmodes of the Dirac operator \mathcal{D} defined by Eq. (2.3) are needed for the quantitative analysis for the relation between confinement and chiral symmetry breaking in QCD. In order to reduce the numerical cost, the technique of the KS formalism for diagonalizing the Dirac operator \mathcal{D} is useful. The KS formalism is originally given by Kogut and Susskind [5]. However, it is applicable to only the even lattice, where all the lattice sizes are even number with the periodic boundary condition. Hence, it is not applicable to the temporally odd-number lattice. However, the KS formalism have been generalized for the temporally odd-number lattice in our study [2]. In the following, we discuss “modified KS formalism” on the temporally odd-number lattice after we review the KS formalism on the even lattice.

The KS formalism is the method for spin-diagonalizing the naive Dirac operator on the lattice. We consider the even lattice, where all the lattice sizes $N_{1\sim 4}$ are even numbers. A matrix $T(s)$ is defined as

$$T(s) \equiv \gamma_1^{s_1} \gamma_2^{s_2} \gamma_3^{s_3} \gamma_4^{s_4}. \quad (2.25)$$

This matrix depends on all the components of the site $s = (s_1, s_2, s_3, s_4)$. Using the matrix, one can diagonalize all the γ -matrices γ_μ ($\mu = 1, 2, 3, 4$);

$$T^\dagger(s) \gamma_\mu T(s \pm \hat{\mu}) = \eta_\mu(s) \mathbf{1}, \quad (2.26)$$

where the staggered phase $\eta_\mu(s)$ is introduced as

$$\eta_1(s) \equiv 1, \quad \eta_\mu(s) \equiv (-1)^{s_1 + \dots + s_{\mu-1}} \quad (\mu \geq 2). \quad (2.27)$$

Note that the Dirac operator $\mathcal{D} = \gamma_\mu D_\mu$ is linear in the γ -matrices. Thus, the Dirac operator is spin-diagonalized as

$$\begin{aligned} \sum_\mu T^\dagger(s) \gamma_\mu D_\mu T(s + \hat{\mu}) \\ = \text{diag}(\eta_\mu D_\mu, \eta_\mu D_\mu, \eta_\mu D_\mu, \eta_\mu D_\mu), \end{aligned} \quad (2.28)$$

where the KS Dirac operator $\eta_\mu D_\mu$ is defined as

$$(\eta_\mu D_\mu)_{ss'} = \frac{1}{2a} \sum_{\mu=1}^4 \eta_\mu(s) [U_\mu(s) \delta_{s+\hat{\mu}, s'} - U_{-\mu}(s) \delta_{s-\hat{\mu}, s'}]. \quad (2.29)$$

From the Eq.(2.28), one can find fourfold degeneracy of the Dirac eigenvalue $i\lambda_n$ relating to the spinor structure of the Dirac operator. Thus, all the eigenvalues of the Dirac operator can be obtained by only solving the KS Dirac eigenvalue equation

$$\eta_\mu D_\mu |n\rangle = i\lambda_n |n\rangle \quad (2.30)$$

where $|n\rangle$ is the KS Dirac eigenstate. Note that the KS Dirac operator has only indices of sites and colors, not spinors. Thus, the numerical cost for solving the KS Dirac eigenvalue equation (2.30) is smaller than that for the Dirac eigenvalue equation (2.7), and the ratio is about 1/16. Using the KS Dirac eigenfunction $\chi_n(s) \equiv \langle s | n \rangle$, the KS Dirac eigenvalue equation (2.30) is explicitly expressed as

$$\begin{aligned} \frac{1}{2a} \sum_{\mu=1}^4 \eta_\mu(s) [U_\mu(s) \chi_n(s + \hat{\mu}) - U_{-\mu}(s) \chi_n(s - \hat{\mu})] \\ = i\lambda_n \chi_n(s). \end{aligned} \quad (2.31)$$

Also, KS Dirac matrix element $\langle n | \hat{U}_\mu | m \rangle$ is expressed as

$$\begin{aligned} \langle n | \hat{U}_\mu | m \rangle &= \sum_s \langle n | s \rangle \langle s | \hat{U}_\mu | s + \hat{\mu} \rangle \langle s + \hat{\mu} | m \rangle \\ &= \sum_s \chi_n(s)^\dagger U_\mu(s) \chi_m(s + \hat{\mu}). \end{aligned} \quad (2.32)$$

Because of fourfold degeneracy of the Dirac eigenvalue, there are four states with the same eigenvalues. These states are labeled with quantum number $I = 1, 2, 3, 4$, namely $|n, I\rangle$ [6]. Using this notation, the Dirac eigenvalue equation (2.7) can be expressed as

$$\not{D} |n, I\rangle = i\lambda_n |n, I\rangle. \quad (2.33)$$

The relation between the Dirac eigenfunction $\psi_n^I(s)_\alpha \equiv \langle s, \alpha | n, I \rangle$ and the spinless KS-Dirac eigenfunction $\chi_n(s)$ is

$$\psi_n^I(s)_\alpha = T(s)_{\alpha I} \chi_n(s). \quad (2.34)$$

The quantum number I is mixed with spinor indices. That can be understood from the fact that the quantum number I comes from the fourfold degeneracy of the Dirac eigenvalue in the spinor space.

At the temporal boundary, the matrix satisfies

$$T(s + N_\tau \hat{4}) = T(s) \gamma_4^{N_\tau}. \quad (2.35)$$

Then, the matrix $T(s)$ is periodic if the temporal length N_τ is even number. Since this situation holds in all the directions, the periodic boundary condition

$$T(s + N_\mu \hat{\mu}) = T(s) \quad (2.36)$$

is satisfied only on the even lattice. Although the spatial periodic boundary condition is not necessarily need physically, the temporal periodic boundary condition is necessary for the imaginary-time finite-temperature formalism. Therefore, the original KS formalism is not applicable to the temporally odd-number lattice.

Note here that this procedure is just a mathematical technique to diagonalize \mathcal{D} , and this never means to use a specific fermion like the KS fermion. In fact, the diagonalization of \mathcal{D} is mathematically equivalent to the use of the KS formalism.

Now, we present the modified KS formalism as the generalization applicable to the temporally odd-number lattice, where the lattice size for temporal direction N_τ is odd number and the lattice sizes for spatial direction N_i ($i = 1, 2, 3$) are even number with the periodic boundary conditions for all the directions.

Instead of the matrix $T(s)$, a matrix $M(s)$ is introduced by

$$M(s) \equiv \gamma_1^{s_1} \gamma_2^{s_2} \gamma_3^{s_3} \gamma_4^{s_1+s_2+s_3}. \quad (2.37)$$

Although the matrix $M(s)$ is similar to the matrix $T(s)$, it is independent of the time component of the site s_4 . Using the matrix $M(s)$, all the γ -matrices are transformed to be proportional to γ_4 :

$$M^\dagger(s) \gamma_\mu M(s \pm \hat{\mu}) = \eta_\mu(s) \gamma_4, \quad (2.38)$$

where $\eta_\mu(s)$ is the staggered phase given by Eq. (2.27). This relation (2.38) is always satisfied for arbitrary representation for the gamma matrices. In the Dirac representation, γ_4 is diagonal as

$$\gamma_4 = \begin{pmatrix} 1 & 0 & 0 & 0 \\ 0 & 1 & 0 & 0 \\ 0 & 0 & -1 & 0 \\ 0 & 0 & 0 & -1 \end{pmatrix} \quad (2.39)$$

and the Dirac representation is taken in this paper. Thus, the Dirac operator $\mathcal{D} = \gamma_\mu D_\mu$ can be spin-diagonalized also on the temporally odd-number lattice:

$$\sum_{\mu} M^{\dagger}(s) \gamma_{\mu} D_{\mu} M(s + \hat{\mu}) = \begin{pmatrix} \eta_{\mu} D_{\mu} & 0 & 0 & 0 \\ 0 & \eta_{\mu} D_{\mu} & 0 & 0 \\ 0 & 0 & -\eta_{\mu} D_{\mu} & 0 \\ 0 & 0 & 0 & -\eta_{\mu} D_{\mu} \end{pmatrix}, \quad (2.40)$$

where $\eta_{\mu} D_{\mu}$ is the KS Dirac operator given in Eq. (2.29).

Note that the modified KS formalism can be applicable to the temporally odd-number lattice. because the periodic boundary condition for the matrix $M(s)$ is satisfied for any direction. In fact, at the temporal boundary,

$$M(s + N_4 \hat{4}) = M(s), \quad (2.41)$$

is trivially satisfied because $M(s)$ is independent of s_4 . Moreover, the spatial boundary conditions for each direction

$$M(s + N_i \hat{i}) = M(s) \quad (i = 1, 2, 3) \quad (2.42)$$

is valid because the spatial lattice sizes are even number. The staggered phase $\eta_{\mu}(s)$ satisfies the periodic boundary condition on the temporally odd-number lattice because the staggered phase $\eta_{\mu}(s)$ is also independent of the time component of the site s_4 . In this way, the KS formalism can be generalized for the temporally odd-number lattice.

The Dirac operator has two positive modes and two negative modes for each eigenvalue λ_n on the temporally odd-number lattice from Eq. (2.40). From the anti-commutator relation (1.14), the existence of the chiral partner $\gamma_5 |n\rangle$ is guaranteed with the eigenvalue $-i\lambda_n$. Thus, also on the temporally odd-number lattice, all the eigenvalues of the Dirac operator can be obtained only by solving the KS Dirac eigenvalue equation (2.31).

In the case of the temporally odd-number lattice, the Dirac eigenstates are labeled with quantum number $I = 1, 2, 3, 4$ according to the spinor structure of the Dirac operator given by Eq. (2.40). These four Dirac eigenfunction $\psi_n^I(s)_{\alpha} \equiv \langle s, \alpha | n, I \rangle$ are constructed For each KS Dirac mode $|n\rangle$ as

$$\psi_n^I(s)_{\alpha} = M(s)_{\alpha I} \chi_n(s). \quad (2.43)$$

The Dirac eigenstates $|n, I\rangle$ have the eigenvalue $i\lambda_n$ with $I = 1, 2$ and have the eigenvalue $-i\lambda_n$ with $I = 3, 4$.

Next, the relation (2.17) is rewritten using the KS Dirac modes. Now the relation (2.17) is correctly written as

$$L = -\frac{(2ai)^{N_{\tau}-1}}{12V} \sum_{n,I} \lambda_n^{N_{\tau}-1} \langle n, I | \hat{U}_4 | n, I \rangle. \quad (2.44)$$

The diagonal Dirac matrix element $\langle n, I | \hat{U}_4 | n, I \rangle$ can be expressed by the diagonal KS Dirac matrix element $\langle n | \hat{U}_4 | n \rangle$:

$$\langle n, I | \hat{U}_4 | n, I \rangle = \langle n | \hat{U}_4 | n \rangle. \quad (2.45)$$

The detailed derivation is shown in the next section. Using the relation (2.45), and taking the structure of the Dirac eigenfunction (2.43) into consideration. RHS of Eq. (2.44) can be rewritten using the KS Dirac modes:

$$\begin{aligned} & \sum_{n,I} \lambda_n^{N_4-1} \langle n, I | \hat{U}_4 | n, I \rangle \\ &= \sum_{n,I=1,2} \lambda_n^{N_4-1} \langle n, I | \hat{U}_4 | n, I \rangle \\ &+ \sum_{n,I=3,4} (-\lambda_n)^{N_4-1} \langle n, I | \hat{U}_4 | n, I \rangle \\ &= \sum_{n,I=1,2,3,4} \lambda_n^{N_4-1} \langle n, I | \hat{U}_4 | n, I \rangle \\ &= \sum_{n,I=1,2,3,4} \lambda_n^{N_4-1} \langle n | \hat{U}_4 | n \rangle \\ &= 4 \sum_n \lambda_n^{N_4-1} \langle n | \hat{U}_4 | n \rangle, \end{aligned} \quad (2.46)$$

where $N_4 - 1$ is even number on the temporally odd-number lattice. Thus, the relation (2.17) is rewritten as

$$L = -\frac{(2ai)^{N_\tau-1}}{3V} \sum_n \lambda_n^{N_\tau-1} \langle n | \hat{U}_4 | n \rangle \quad (2.47)$$

using the modified KS formalism. Note that the (modified) KS formalism is an exact mathematical method for spin-diagonalizing the Dirac operator, not an approximation. Thus Eqs. (2.44) and (2.47) are exactly equivalent. Therefore, each Dirac-mode contribution to the Polyakov loop can be obtained by solving the eigenvalue equation of the KS Dirac operator whose dimension is $(N_c \times V)^2$ instead of the original Dirac operator whose dimension is $(4 \times N_c \times V)^2$ on the temporally odd-number lattice.

Note again that a specific fermion like the KS fermion is not used. We just use the KS formalism for diagonalizing the naive Dirac operator \not{D} defined by Eq. (2.3), and obtain all the eigenvalues and the eigenfunctions. Actually, all the eigenvalues and eigenfunctions can be obtained without the KS formalism by the direct diagonalization of the Dirac operator \not{D} , and they gives the same results. however, the numerical cost is larger.

2.1.5 The Relation Between the Dirac Matrix Element and the KS Dirac Matrix Element

The relations between the Dirac matrix element and the KS Dirac matrix element are shown in both even and temporally odd-number lattices.

First, the even lattice and the original KS formalism is considered. Using the relation between the Dirac eigenfunction ψ and the KS-Dirac eigenfunction χ , the Dirac matrix element of a link variable operator $\langle n, I | \hat{U}_\mu | m, J \rangle$ is expressed as

$$\begin{aligned}
 \langle n, I | \hat{U}_\mu | m, J \rangle &= \sum_{s, \alpha} \psi_n^I(s)_\alpha^\dagger U_\mu(s) \psi_m^J(s + \hat{\mu})_\alpha \\
 &= \sum_{s, \alpha} \chi_n(s)^\dagger T^\dagger(s)_{I\alpha} U_\mu(s) T(s + \hat{\mu})_{\alpha J} \chi_m(s + \hat{\mu}) \\
 &= \sum_s \chi_n(s)^\dagger \{ T^\dagger(s) T(s + \hat{\mu}) \}_{IJ} U_\mu(s) \chi_m(s + \hat{\mu}). \tag{2.48}
 \end{aligned}$$

From the direct calculation, the matrix $T^\dagger(s) T(s + \hat{\mu})$ is calculated from the definition of the matrix $T(s)$ (2.25):

$$T^\dagger(s) T(s + \hat{\mu}) = \tilde{\eta}_\mu^{(E)}(s) \gamma_\mu, \tag{2.49}$$

where $\tilde{\eta}_\mu^{(E)}(s)$ is a sign function defined as

$$\tilde{\eta}_\mu^{(E)}(s) = (-1)^{s_{\mu+1} + \dots + s_4} \quad (\mu \leq 3), \quad \tilde{\eta}_4^{(E)}(s) = 1, \tag{2.50}$$

which is similar to the staggered phase (2.27). Then, the Dirac matrix element is expressed as

$$\begin{aligned}
 \langle n, I | \hat{U}_\mu | m, J \rangle &= (\gamma_\mu)_{IJ} \sum_s \tilde{\eta}_\mu^{(E)}(s) \chi_n(s)^\dagger U_\mu(s) \chi_m(s + \hat{\mu}) \\
 &= (\gamma_\mu)_{IJ} (n | \hat{\tilde{\eta}}_\mu^{(E)} \hat{U}_\mu | m), \tag{2.51}
 \end{aligned}$$

where $\hat{\tilde{\eta}}_\mu^{(E)}$ is an operator defined as

$$\langle s | \hat{\tilde{\eta}}_\mu^{(E)} | s' \rangle = \tilde{\eta}_\mu^{(E)}(s) \delta_{ss'} \tag{2.52}$$

corresponding to the sign function $\tilde{\eta}_\mu^{(E)}(s)$. In particular, since $\tilde{\eta}_4^{(E)}(s) = 1$ is satisfied for $\mu = 4$, we obtain

$$\langle n, I | \hat{U}_4 | m, J \rangle = (\gamma_4)_{IJ} \langle n | \hat{U}_4 | m \rangle. \quad (2.53)$$

Here we consider only the Dirac matrix element of one link-variable operator $\langle n, I | \hat{U}_\mu | m, J \rangle$. However, that of other operator consisting of link-variable operators $\langle n, I | \hat{O}(\hat{U}) | m, J \rangle$ can be evaluated in terms of the KS Dirac matrix element or the KS Dirac eigenfunction $\chi_n(s)$ by similar calculation on the even lattice.

Next, the temporally odd-number lattice and the modified KS formalism are considered. Corresponding to the even lattice, the Dirac matrix element of a link variable operator $\langle n, I | \hat{U}_\mu | m, J \rangle$ is expressed as

$$\begin{aligned} \langle n, I | \hat{U}_\mu | m, J \rangle &= \sum_{s, \alpha} \psi_n^I(s)_\alpha^\dagger U_\mu(s) \psi_m^J(s + \hat{\mu})_\alpha \\ &= \sum_{s, \alpha} \chi_n(s)^\dagger M^\dagger(s)_{I\alpha} U_\mu(s) M(s + \hat{\mu})_{\alpha J} \chi_m(s + \hat{\mu}) \\ &= \sum_s \chi_n(s)^\dagger \{ M^\dagger(s) M(s + \hat{\mu}) \}_{IJ} U_\mu(s) \chi_m(s + \hat{\mu}) \end{aligned} \quad (2.54)$$

Like the case of the Eq. (2.49), $M^\dagger(s) M(s + \hat{\mu})$ can be calculated as

$$M^\dagger(s) M(s + \hat{\mu}) = \tilde{\eta}_\mu^{(O)}(s) \gamma_\mu \gamma_4, \quad (2.55)$$

where $\tilde{\eta}_\mu^{(O)}(s)$ is a different sign function defined as

$$\tilde{\eta}_\mu^{(O)}(s) = (-1)^{s_1 + \dots + s_\mu} \quad (\mu \leq 3), \quad \tilde{\eta}_4^{(O)}(s) = 1. \quad (2.56)$$

Using this fact, the Dirac matrix element can be written as

$$\begin{aligned} \langle n, I | \hat{U}_\mu | m, J \rangle &= (\gamma_\mu \gamma_4)_{IJ} \sum_s \tilde{\eta}_\mu^{(O)}(s) \chi_n(s)^\dagger U_\mu(s) \chi_m(s + \hat{\mu}) \\ &= (\gamma_\mu \gamma_4)_{IJ} \langle n | \hat{\tilde{\eta}}_\mu^{(O)} \hat{U}_\mu | m \rangle, \end{aligned} \quad (2.57)$$

where $\hat{\tilde{\eta}}_\mu^{(O)}$ is an operator defined as

$$\langle s | \hat{\tilde{\eta}}_\mu^{(O)} | s' \rangle = \tilde{\eta}_\mu^{(O)}(s) \delta_{ss'} \quad (2.58)$$

corresponding to the sign function $\tilde{\eta}_\mu^{(E)}(s)$. In particular, since $\tilde{\eta}_4^{(O)}(s) = 1$ is satisfied for $\mu = 4$, we obtain

$$\langle n, I | \hat{U}_4 | m, J \rangle = \delta_{IJ} \langle n | \hat{U}_4 | m \rangle. \quad (2.59)$$

For more special case, the diagonal component $\langle n, I | \hat{U}_4 | n, I \rangle$ is expressed as

$$\langle n, I | \hat{U}_4 | n, I \rangle = \langle n | \hat{U}_4 | n \rangle. \quad (2.60)$$

This is used in Chap. 2 in this thesis.

Like the case of the even lattice, one can evaluate the Dirac matrix element of the other operator $\langle n, I | \hat{O}(\hat{U}) | m, J \rangle$, using the KS Dirac matrix element or the KS Dirac eigenfunction $\chi_n(s)$ on the temporally odd-number lattice.

2.1.6 Numerical Analysis

Next, the numerical analysis is shown for the relation between confinement and chiral symmetry breaking in QCD based on the relation (2.47) connecting the Polyakov loop and Dirac modes on the temporally-odd number lattice. The eigenvalue and eigenfunction of the KS Dirac operator is obtained by using the Linear Algebra PACKage (LAPACK) [7].

The SU(3) lattice QCD Monte Carlo simulations are performed at the quenched level with the standard Wilson plaquette action in both cases of confinement and deconfinement phases. The lattice setup is $10^3 \times 5$ with $\beta \equiv \frac{2N_c}{g^2} = 5.6$ (i.e., $a \simeq 0.25$ fm), and $10^3 \times 3$ with $\beta = 5.7$ (i.e., $a \simeq 0.20$ fm). The former corresponds to $T \equiv 1/(N_\tau a) \simeq 160$ MeV, and it describes the confinement phase. The latter corresponds to $T \equiv 1/(N_\tau a) \simeq 330$ MeV, and it describes the deconfinement phase. 20 gauge configurations are used for each phase, and they are taken every 500 sweeps after the thermalization of 5,000 sweeps.

In order to confirm that the relation (2.47) is satisfied numerically, we have independently calculated LHS and RHS of the relation (2.47) and compare them. The numerical results for each gauge-configuration in both confinement and deconfinement phases are shown in Tables 2.1 and 2.2, respectively.

From Tables 2.1 and 2.2, it is found that Eq. (2.47) is exactly valid for each gauge configuration in both confinement and deconfinement phases as expected above. In fact, the Elitzur's theorem is not necessary for the derivation of the relation because it is satisfied for each gauge-configuration. Then, we can quantitatively investigate the relation between confinement and chiral symmetry breaking in QCD using the relation (2.47) with a single gauge-configuration.

In the deconfinement phase, the Z_3 center symmetry at the quenched level is spontaneously broken, and the Polyakov loop is proportional to $e^{i\frac{2\pi}{3}k}$ ($k = 0, \pm 1$) for each gauge configuration [6]. In this paper, the vacuum where the Polyakov loop is almost real ($j = 0$) is referred to as the “real Polyakov-loop vacuum” and the other vacua is called as the “ Z_3 -rotated vacua.” At the quenched level, it is numerically confirmed that the relation (2.47) is exactly satisfied in the Z_3 -rotated vacua as well as the real Polyakov-loop vacuum.

Table 2.1 Numerical results for LHS and RHS of the relation (2.47) on the $10^3 \times 5$ lattice with $\beta = 5.6$ for each gauge configuration, where the system is in confinement phase. L_D is defined as the R.H.S of the relation (2.47). This table is essentially same as that in Ref. [2]

Configuration No.	$\text{Re}L$	$\text{Im}L$	$\text{Re}L_D$	$\text{Im}L_D$
1	0.00961	-0.00322	0.00961	-0.00322
2	-0.00161	-0.00125	-0.00161	-0.00125
3	0.0139	-0.00438	0.0139	-0.00438
4	-0.00324	-0.00519	-0.00324	-0.00519
5	0.000689	-0.0101	0.000689	-0.0101
6	0.00423	-0.0168	-0.00423	-0.0168
7	-0.00807	-0.00265	-0.00807	-0.00265
8	-0.00918	-0.00683	-0.00918	-0.00683
9	0.00624	-0.00448	0.00624	-0.00448
10	-0.00437	0.00700	-0.00437	0.00700

Table 2.2 Numerical results for LHS and RHS of the relation (2.47) on the $10^3 \times 3$ lattice with $\beta = 5.7$ for each gauge configuration, where the system is in deconfinement phase. This table is essentially same as that in Ref. [2]

Configuration No.	$\text{Re}L$	$\text{Im}L$	$\text{Re}L_D$	$\text{Im}L_D$
1	0.316	-0.00104	0.316	-0.00104
2	0.337	-0.00597	0.337	-0.00597
3	0.331	0.00723	0.331	0.00723
4	0.305	-0.00334	0.305	-0.00334
5	0.313	0.00167	0.314	0.00167
6	0.316	0.000120	0.316	0.000120
7	0.337	0.000482	0.337	0.000482
8	0.300	-0.00690	0.300	-0.00690
9	0.344	-0.00102	0.344	-0.00102
10	0.347	-0.00255	0.347	-0.00255

In the case of the full QCD calculations, where dynamical quarks are included, the real Polyakov-loop vacuum is selected as the stable vacuum, and the Z_3 -rotated vacua are meta-stable states. Then, the real Polyakov-loop vacuum would be more significant than other vacua in the deconfinement phase. Even in full QCD, the mathematical relation (2.47) is exact because it is not related to how the link-variables are generated.

Next, we numerically investigate each Dirac-mode contribution in order to confirm that the low-lying Dirac modes have negligible contribution to the Polyakov loop

based on the relation (2.47). This is expected from the analytical relation (2.47) as discussed above, however, the quantitative numerical analysis is also meaningful.

Since RHS of the Eq. (2.47) is expressed as a sum over the Dirac-mode contribution, the individual contribution to the Polyakov loop from each Dirac mode. Then, the Polyakov loop without low-lying Dirac-mode contribution is introduced as

$$L_{\text{IR-cut}} = -\frac{(2ai)^{N_\tau-1}}{3V} \sum_{|\lambda_n| > \Lambda_{\text{IR}}} \lambda_n^{N_\tau-1} (n | \hat{U}_4 | n), \quad (2.61)$$

where Λ_{IR} is the infrared (IR) cutoff for Dirac eigenvalue λ_n . The chiral condensate $\langle \bar{q}q \rangle$ is expressed on the lattice as

$$\begin{aligned} \langle \bar{q}q \rangle &= -\frac{1}{V} \text{Tr}_{c,\gamma} \frac{1}{\not{D} + m} \\ &= -\frac{1}{V} \sum_n \frac{1}{i\lambda_n + m} \\ &= -\frac{1}{V} \left(\sum_{\lambda_n > 0} \frac{2m}{\lambda_n^2 + m^2} + \frac{\nu}{m} \right), \end{aligned} \quad (2.62)$$

where m is the current quark mass and ν the total number of zero modes of \not{D} .

In Fig. 2.3, the Dirac eigenvalue distribution $\rho(\lambda)$ in confinement and deconfinement phases are shown. In the deconfinement phase, the density of low-lying Dirac-modes is small and $\rho(\lambda = 0) \simeq 0$. It means that the chiral condensate is almost zero and the chiral symmetry is restored. Then, in the deconfinement phase, the effect of low-lying Dirac-modes to the Polyakov loop might not be interesting because low-lying Dirac-modes are almost absent.

After the removal of contribution from the low-lying Dirac modes below IR cutoff Λ_{IR} , the chiral condensate is written as

$$\langle \bar{q}q \rangle_{\Lambda_{\text{IR}}} = -\frac{1}{V} \sum_{\lambda_n \geq \Lambda_{\text{IR}}} \frac{2m}{\lambda_n^2 + m^2} \quad (2.63)$$

In this thesis, the IR cutoff is set as $\Lambda_{\text{IR}} \simeq 0.4 \text{ GeV}$. In the confined phase, using this IR Dirac-mode cut, chiral-symmetry is almost restored, and the chiral condensate is strongly reduced as

$$\frac{\langle \bar{q}q \rangle_{\Lambda_{\text{IR}}}}{\langle \bar{q}q \rangle} \simeq 0.02 \quad (2.64)$$

in the case of physical current-quark mass, $m \simeq 5 \text{ MeV}$ [1].

For 10 gauge configurations, the numerical results for L and $L_{\text{IR-cut}}$ in both confinement and deconfinement phases are shown in Tables 2.3 and 2.4, respectively.

Fig. 2.3 The lattice QCD result for the Dirac eigenvalue distribution $\rho(\lambda)$ in confinement and deconfinement phases in the lattice unit. The *upper figure* is the results on $10^3 \times 5$ lattice with $\beta = 5.6$ (i.e., $a \simeq 0.25$ fm), where the system is in the confinement phase. The *lower figure* is the results on $10^3 \times 5$ lattice with $\beta = 6.0$ (i.e., $a \simeq 0.10$ fm). Where the system is in the deconfinement phase. These figures are taken from Ref. [2]

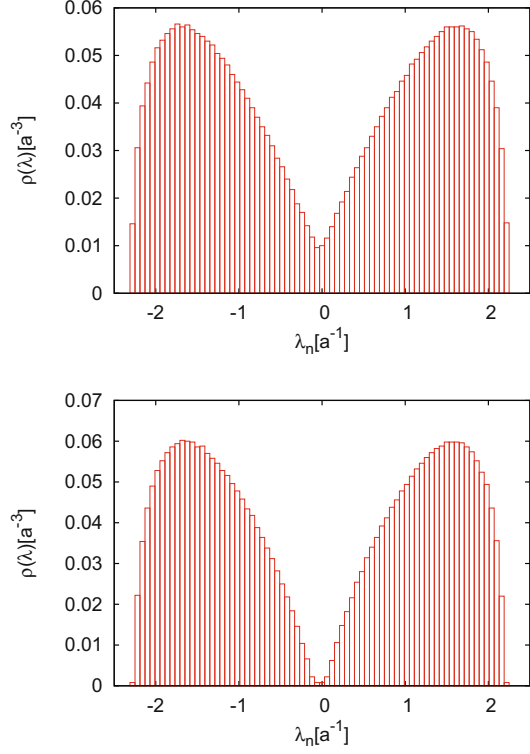


Table 2.3 Numerical results for L and $L_{\text{IR-cut}}$ on the $10^3 \times 5$ lattice with $\beta = 5.6$ for each gauge configuration, where the system is in confinement phase. This table is essentially same as that in Ref. [2]

Configuration No.	$\text{Re}L$	$\text{Im}L$	$\text{Re}L_{\text{IR-cut}}$	$\text{Im}L_{\text{IR-cut}}$
1	0.00961	-0.00322	0.00961	-0.00321
2	-0.00161	-0.00125	-0.00160	-0.00125
3	0.0139	-0.00438	0.0139	-0.00437
4	-0.00324	-0.00519	-0.00325	-0.00520
5	0.000689	-0.0101	0.000706	-0.0101
6	0.00423	-0.0168	0.00422	-0.0168
7	-0.00807	-0.00265	-0.00807	-0.00264
8	-0.00918	-0.00683	-0.00918	-0.00682
9	0.00624	-0.00448	0.00624	-0.00448
10	-0.00437	0.00700	-0.00436	0.00698

Table 2.4 Numerical results for L and $L_{\text{IR-cut}}$ on the $10^3 \times 3$ lattice with $\beta = 5.7$ for each gauge configuration, where the system is in deconfinement phase. This table is essentially same as that in Ref. [2]

Configuration No.	Re L	Im L	Re $L_{\text{IR-cut}}$	Im $L_{\text{IR-cut}}$
1	0.316	-0.00104	0.319	-0.00103
2	0.337	-0.00597	0.340	-0.00597
3	0.331	0.00723	0.334	0.00724
4	0.305	-0.00334	0.307	-0.00333
5	0.314	0.00167	0.317	0.00167
6	0.316	0.000120	0.319	0.000121
7	0.337	0.0000482	0.340	0.0000475
8	0.300	-0.00690	0.303	-0.00691
9	0.344	-0.00102	0.347	-0.00102
10	0.347	-0.00255	0.350	-0.00256

From Tables 2.3 and 2.4, it is found that

$$L \simeq L_{\text{IR-cut}} \quad (2.65)$$

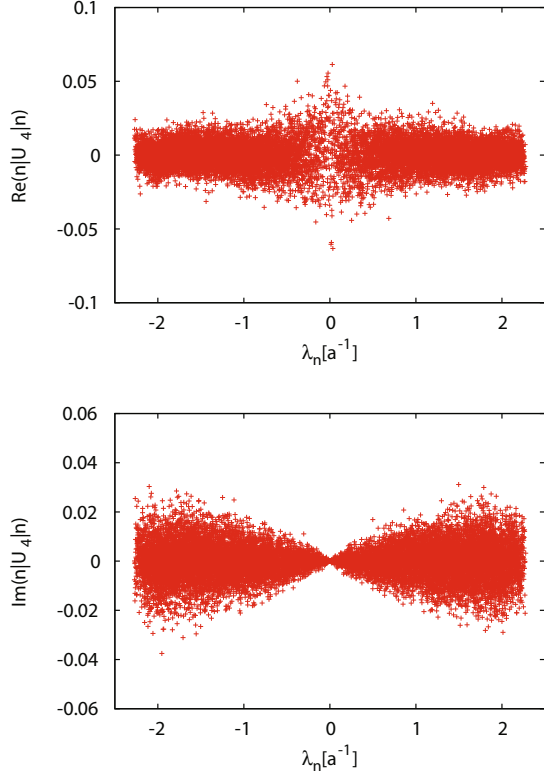
is almost satisfied for each gauge configuration in both confinement and deconfinement phases. In the deconfinement phase, we have confirmed that $L \simeq L_{\text{IR-cut}}$ is valid for both real Polyakov-loop vacuum and Z_3 -rotated vacua. Thus, the configuration average $\langle L \rangle \simeq \langle L_{\text{IR-cut}} \rangle$ is of course almost satisfied. Therefore, the low-lying Dirac modes have negligible contribution to the Polyakov loop. This results suggest that the low-lying Dirac modes below the IR cutoff $|\lambda_n| < \Lambda_{\text{IR}} \simeq 0.4 \text{ GeV}$ are not essential for confinement while they are essential for chiral symmetry breaking from Eq. (2.64). Thus, our results indicate that there is no direct one-to-one correspondence between confinement and chiral symmetry breaking in QCD.

2.1.7 New “positive/negative Symmetry” on Dirac Matrix Element in Confinement Phase

We investigate the properties of the matrix element $\langle n | \hat{U}_4 | n \rangle$ and each Dirac-mode contribution $\lambda_n^{N_\tau-1} \langle n | \hat{U}_4 | n \rangle$ in both confinement and deconfinement phases. The Polyakov loop is obtained by multiplying all the sum of each Dirac-mode contribution $\sum_n \lambda_n^{N_\tau-1} \langle n | \hat{U}_4 | n \rangle$ by the overall factor $-(2ai)^{N_\tau-1}/(3V)$ in Eq. (2.47).

In Fig. 2.4, the numerical results for the matrix elements $\text{Re}(\langle n | \hat{U}_4 | n \rangle)$ and $\text{Im}(\langle n | \hat{U}_4 | n \rangle)$ in confinement phase are shown. They are plotted against Dirac eigenvalues λ_n in the lattice unit for one gauge configuration. In Fig. 2.5, each Dirac-mode contribution to the Polyakov loop $\lambda_n^{N_\tau-1} \text{Re}(\langle n | \hat{U}_4 | n \rangle)$ and $\lambda_n^{N_\tau-1} \text{Im}(\langle n | \hat{U}_4 | n \rangle)$ are shown

Fig. 2.4 The numerical results for the real part $\text{Re}(n|\hat{U}_4|n)$ and the imaginary part $\text{Im}(n|\hat{U}_4|n)$ of the KS-Dirac matrix element in the confinement phase, plotted against the Dirac eigenvalue λ_n in the lattice unit on $10^3 \times 5$ with $\beta = 5.6$. One can find the positive/negative symmetry in the distributions. These figures are taken from Ref. [2]

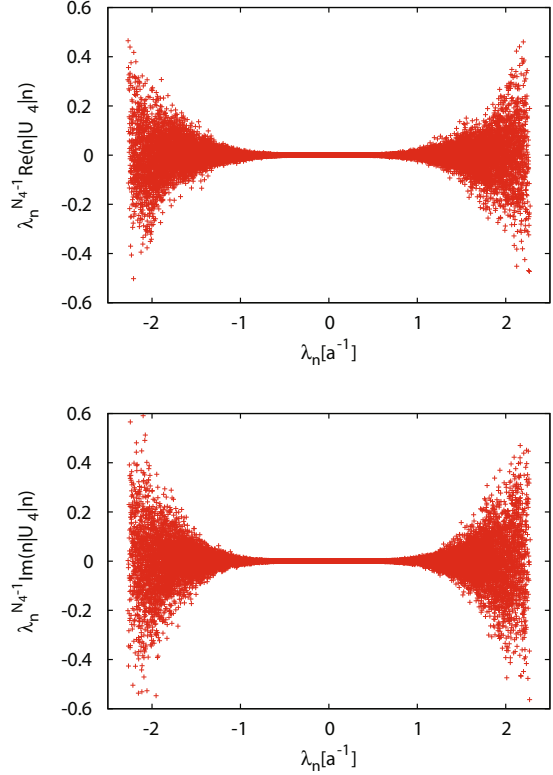


in the confinement phase. They are plotted against Dirac eigenvalues λ_n in the lattice unit. From Fig. 2.4, it is found that the real part of the matrix element $\text{Re}(n|\hat{U}_4|n)$ is generally nonzero in the confinement phase, and it is not small in low-lying Dirac-mode region with $|\lambda_n| \sim 0$. However, from Fig. 2.5, it is directly confirmed that the Dirac-mode contribution to the Polyakov loop, $\lambda_n^{N_\tau-1} \text{Re}(n|\hat{U}_4|n)$, is small in low-lying Dirac-mode region thanks to the damping factor $\lambda_n^{N_\tau-1}$. Thus, the damping factor $\lambda_n^{N_\tau-1}$ plays an important role in the Eq. (2.47).

On the other hand, from Fig. 2.4, the imaginary part $\text{Im}(n|\hat{U}_4|n)$ of the matrix element is relatively small in low-lying Dirac-mode region unlike the case of the real part, $\text{Re}(n|\hat{U}_4|n)$. However, as shown in Fig. 2.5, the low-lying Dirac mode contribution to the imaginary part of the Polyakov loop, $\lambda_n^{N_\tau-1} \text{Im}(n|\hat{U}_4|n)$ is small.

As a remarkable feature, from Fig. 2.4, one can find a new symmetry of “positive/negative symmetry” in the distribution of Dirac-mode matrix element $(n|\hat{U}_4|n)$, namely $\text{Re}(n|\hat{U}_4|n)$ and $\text{Im}(n|\hat{U}_4|n)$ in the confinement phase. Since the damping factor trivially has the same symmetry, the distribution of each Dirac-mode contribution to the Polyakov loop, $\lambda_n^{N_\tau-1} (n|\hat{U}_4|n)$, has the same symmetry. The Polyakov loop is proportional to all the sum of each Dirac-mode contribution to the Polyakov loop, and the zero-value of the Polyakov loop $\langle L \rangle = 0$ comes from the new symmetry in

Fig. 2.5 The numerical results for each Dirac-mode contribution to the Polyakov loop, $\lambda_n^{N_\tau-1} \text{Re}(n|\hat{U}_4|n)$ and $\lambda_n^{N_\tau-1} \text{Im}(n|\hat{U}_4|n)$ in the confinement phase, plotted against the Dirac eigenvalue λ_n in the lattice unit on $10^3 \times 5$ with $\beta = 5.6$. These figures are taken from Ref. [2]



the confinement phase. Moreover, due to the symmetry in the confinement phase, the contribution to the Polyakov loop from arbitrary Dirac-mode region $\Lambda_1 \leq \lambda_n \leq \Lambda_2$ is zero:

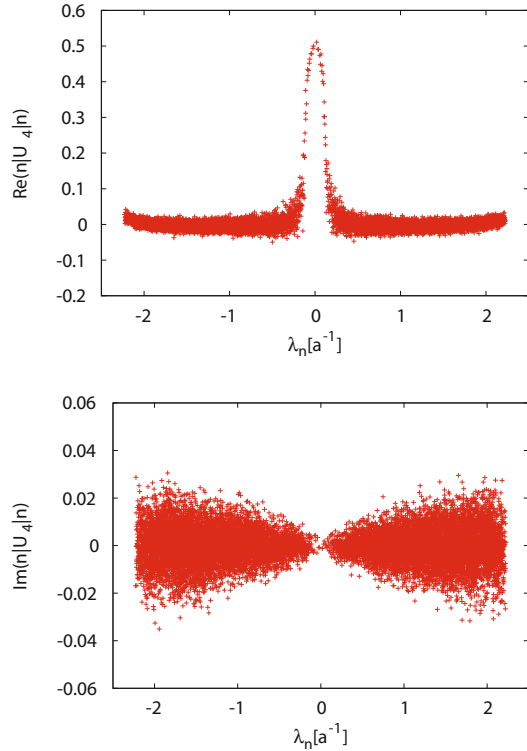
$$\sum_{\Lambda_1 \leq \lambda_n \leq \Lambda_2} \lambda_n^{N_\tau-1} (n|\hat{U}_4|n) = 0 \quad (\text{in the confinement phase}). \quad (2.66)$$

This behavior in the confinement phase is consistent with the previous works [1, 8].

Since quarks are deconfined and the chiral symmetry is restored in the deconfinement phase, it might be less interesting to consider their relation. In the following, only the real Polyakov-loop vacuum is considered because it is selected as the stable vacuum in full QCD.

In Figs. 2.6 and 2.7, the matrix elements $(n|\hat{U}_4|n)$ and each Dirac-mode contribution $\lambda_n^{N_\tau-1} \text{Re}(n|\hat{U}_4|n)$ in the deconfinement phase with real Polyakov loop. They are plotted against the Dirac eigenvalue λ_n . Since the imaginary part of the Polyakov loop is also zero in the real Polyakov-loop vacuum, the imaginary part $\text{Im}(n|\hat{U}_4|n)$ of the matrix element shows the same behavior as the case of the confinement phase. (Compare Figs. 2.4b and 2.6b.) Then, only the results for real part of these quantities

Fig. 2.6 The numerical results for the real part $\text{Re}(n|\hat{U}_4|n)$ and the imaginary part $\text{Im}(n|\hat{U}_4|n)$ of the KS-Dirac matrix element in the real Polyakov-loop vacuum in the deconfinement phase, plotted against the Dirac eigenvalue λ_n in the lattice unit on $10^3 \times 3$ with $\beta = 5.7$. There is no positive/negative symmetry in the distribution of the real part $\text{Re}(n|\hat{U}_4|n)$ unlike the confinement phase. These figures are taken from Ref. [2]

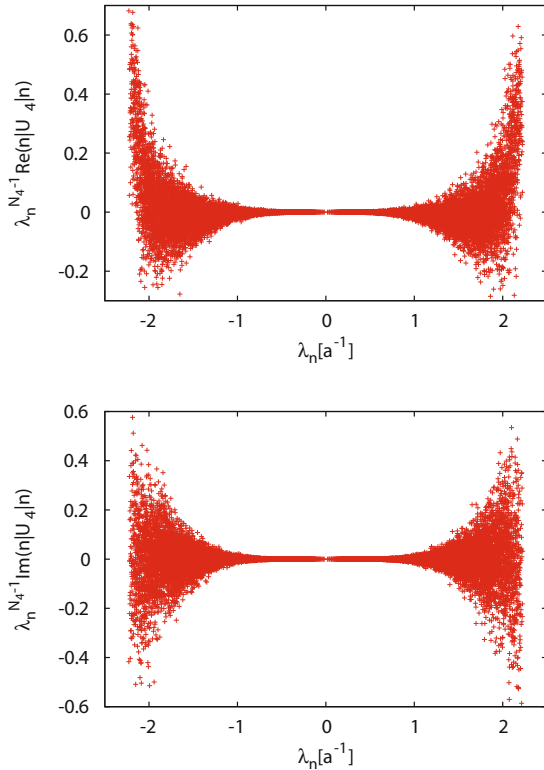


are considered in the deconfinement phase. The results for a single gauge configuration are shown like the case of the confinement phase because the results show almost same behavior as the other configuration.

From Fig. 2.6, one can find a peak structure in the distribution of the real part $\text{Re}(n|\hat{U}_4|n)$ of the matrix element in the low-lying mode region. However, like the case of the confinement phase, from Fig. 2.7, each Dirac-mode contribution $\lambda_n^{N_\tau-1} \text{Re}(n|\hat{U}_4|n)$ is relatively small in low-lying Dirac-mode region due to the damping factor $\lambda_n^{N_\tau-1}$. More quantitatively, from Fig. 2.7, since the distribution of the matrix element in the intermediate region is almost symmetric, only the high-lying Dirac modes have nonzero contribution to the Polyakov loop.

In the deconfinement phase, there is no more positive/negative symmetry for the distributions of the matrix element $(n|\hat{U}_4|n)$ and each Dirac-mode contribution $\lambda_n^{N_\tau-1} (n|\hat{U}_4|n)$, unlike the case of the confinement phase with the symmetry. The Polyakov loop is nonzero because of the asymmetry in the distribution of the matrix element and each Dirac-mode contribution, while the Polyakov loop in the confinement phase is zero because of the symmetry. Thus, the appearance of the positive/negative symmetry on the matrix element $(n|\hat{U}_4|n)$ is strongly related to deconfinement phase transition. This behavior is similar to the Z_3 center symmetry, which is not broken in the confinement phase and is broken in the deconfinement

Fig. 2.7 The numerical results for each Dirac-mode contribution to the Polyakov loop, $\lambda_n^{N_\tau-1} \text{Re}(n|\hat{U}_4|n)$ and $\lambda_n^{N_\tau-1} \text{Im}(n|\hat{U}_4|n)$, in the real Polyakov-loop vacuum in the deconfinement phase plotted against the Dirac eigenvalue λ_n in the lattice unit on $10^3 \times 3$ with $\beta = 5.7$. These figures are taken from Ref. [2]



phase at the quenched level. Therefore, it is interesting to investigate the relation between the new positive/negative symmetry and the Z_3 center symmetry.

2.2 Polyakov Loop Fluctuations

In this section, we will improve the discussion on the relation between the Polyakov loop and the Dirac modes by considering the Polyakov loop fluctuations [9]. In fact, there are 2 reasons to consider the Polyakov loop fluctuations. One is the correctness of the order parameter for the deconfinement and the other is the ambiguity for the renormalization of the Polyakov loop.

The pure $SU(3)$ gauge theory corresponds to the quenched QCD, quarks are treated as the heavy probes. However, the theory interested is the real QCD where quark masses are small. If the quark is light, the behavior of the Polyakov loop changes due to the explicit breaking of the Z_3 center symmetry. On the one hand, the Polyakov loop is an exact order parameter of the Z_3 center symmetry and for deconfinement, which leads a first order phase transition in the quenched QCD [6, 10–12]. On the

other hand, in the presence of light dynamical quarks, the Polyakov loop is no longer an order parameter for the deconfinement transition and is smoothly changing with temperature [13–17]. Then, it will be shown that particular ratios of the Polyakov loop susceptibilities reflect the underlying Z_3 center symmetry and can serve as observables to identify the onset of deconfinement in QCD.

In the lattice QCD, the ultraviolet (UV) divergence of the free energy of bare quark in the continuum limit, and then the bare Polyakov loop vanishes at any temperature. Thus, the Polyakov loop must be renormalized so that it has a physically meaningful continuum limit. However, the renormalization of gluon correlation functions in general, and the Polyakov loop susceptibility in particular, still has uncertainties. Then, it will be that the ambiguities of the renormalization of the Polyakov loop are partially canceled in particular ratios of the Polyakov loop susceptibilities.

After we review the properties of the Polyakov loop fluctuations, and investigate the relation between confinement and chiral symmetry breaking in terms of the Polyakov loop fluctuations and their ratios. We derive the analytic relations between the real, imaginary and modulus of the Polyakov loop and their fluctuations and the Dirac modes on the temporally odd-number lattice with the periodic boundary condition. Then, we particularly consider the contribution of the low-lying Dirac modes to the Polyakov loop fluctuations.

2.2.1 Properties of Polyakov Loop Fluctuations

For each gauge configuration, by operating the Z_3 rotation the Polyakov loop (2.10), the Z_3 rotated Polyakov loop L is defined as

$$\tilde{L} = L e^{2\pi k i/3} \quad (2.67)$$

with $k = 0, \pm 1$ [18, 19]. The variable k is determined so that $k = 0$ in the confined phase is taken, and k in the deconfined phase is taken such that the transformed Polyakov loop \tilde{L} lies in its real sector. Using the Z_3 rotated Polyakov loop and its absolute value, the Polyakov loop susceptibilities are defined as

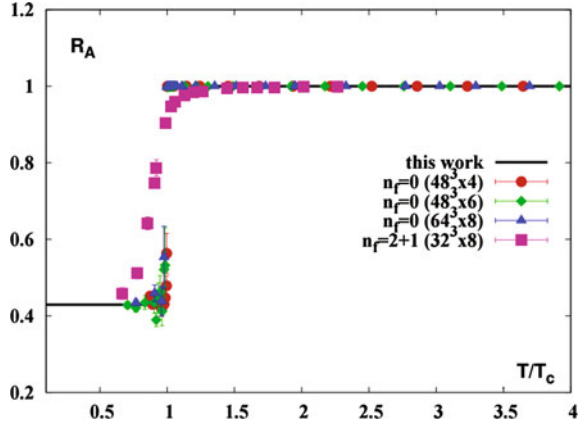
$$T^3 \chi_A = \frac{N_\sigma^3}{N_\tau^3} [\langle |L|^2 \rangle - \langle |L| \rangle^2], \quad (2.68)$$

$$T^3 \chi_L = \frac{N_\sigma^3}{N_\tau^3} [\langle (L_L)^2 \rangle - \langle L_L \rangle^2], \quad (2.69)$$

$$T^3 \chi_T = \frac{N_\sigma^3}{N_\tau^3} [\langle (L_T)^2 \rangle - \langle L_T \rangle^2], \quad (2.70)$$

where $L_L \equiv \text{Re}(\tilde{L})$ and $L_T \equiv \text{Im}(\tilde{L})$, and consider their ratios,

Fig. 2.8 The temperature dependence of the ratio R_A . The lattice QCD simulations are performed at the quenched level and with the physical dynamical quarks. The temperature T is normalized by the deconfinement temperature T_c . The figure is taken from Ref. [19]



$$R_A \equiv \frac{\chi_A}{\chi_L}, \quad (2.71)$$

$$R_T \equiv \frac{\chi_T}{\chi_L}. \quad (2.72)$$

In particular, the ratio (2.71) of the Polyakov loop susceptibilities is important quantity. It is numerically shown to be robust probes of the deconfinement transition, shown in Fig. 2.8. It is almost temperature independent above and below the transition and there is a rapid change near the chiral crossover $T \simeq 150$. This characteristic behavior is understood in terms of the global Z_3 symmetry of the Yang-Mills Lagrangian and the general properties of the Polyakov loop probability distribution [18]. Moreover, the ambiguities of the renormalization of the Polyakov loop are partially canceled in the ratios. In fact, when renormalization of the Polyakov loop is multiplicative renormalization

$$L^{\text{ren}} = Z(g^2)L, \quad (2.73)$$

the renormalization function $Z(g^2)$ is canceled in the ratios. Therefore, the ratios of the Polyakov loop susceptibilities are superior to the Polyakov loop itself.

In the following, we derive the analytical relations between the Polyakov loop fluctuations and the Dirac eigenmodes on the temporally odd-number lattice. And then, we both analytically and numerically investigate the contributions of the low-lying Dirac modes to the Polyakov loop fluctuation ratios.

2.2.2 The Polyakov Loop Fluctuations and Dirac Modes

Next, we derive the relations between the Polyakov loop fluctuations and the Dirac modes. For simplicity, we consider the temporally odd-number lattice. We start the

relation between the Polyakov loop and the Dirac modes (2.17). Since Eq. (2.17) is satisfied for each gauge-configuration, one can find the relation between the Z_3 transformed Polyakov loop \tilde{L} and the Dirac modes,

$$\tilde{L} = \frac{(2ai)^{N_\tau-1}}{12V} \sum_n \lambda_n^{N_\tau-1} e^{2\pi ki/3} \langle n | \hat{U}_4 | n \rangle, \quad (2.74)$$

by multiplying Eq. (2.17) by the Z_3 factor $e^{2\pi ki/3}$. Then, taking the real and the imaginary parts of Eq. (2.74), the longitudinal and transverse Polyakov loops can be expressed as

$$L_L = \frac{(2ai)^{N_\tau-1}}{12V} \sum_n \lambda_n^{N_\tau-1} \text{Re} \left(e^{2\pi ki/3} \langle n | \hat{U}_4 | n \rangle \right), \quad (2.75)$$

$$L_T = \frac{(2ai)^{N_\tau-1}}{12V} \sum_n \lambda_n^{N_\tau-1} \text{Im} \left(e^{2\pi ki/3} \langle n | \hat{U}_4 | n \rangle \right), \quad (2.76)$$

respectively. Also, by taking the absolute value of Eq. (2.17), the absolute value of the Polyakov loop can be written as

$$|L| = \frac{(2a)^{N_\tau-1}}{12V} \left| \sum_n \lambda_n^{N_\tau-1} \langle n | \hat{U}_4 | n \rangle \right|. \quad (2.77)$$

Since Eqs. (2.74), (2.75), (2.76) and (2.77) are satisfied for each gauge configuration, the relations between them and the Dirac eigenmodes by substituting Eqs. (2.75)–(2.77) to Eqs. (2.68)–(2.70). In particular, the Dirac spectral representation of the $R_A = \chi_A/\chi_L$ ratio is expressed as

$$R_A = \frac{\left\langle \left| \sum_n \lambda_n^{N_\tau-1} \langle n | \hat{U}_4 | n \rangle \right|^2 \right\rangle - \left\langle \left| \sum_n \lambda_n^{N_\tau-1} \langle n | \hat{U}_4 | n \rangle \right| \right\rangle^2}{\left\langle \left(\sum_n \lambda_n^{N_\tau-1} \text{Re} \left(e^{2\pi ki/3} \langle n | \hat{U}_4 | n \rangle \right) \right)^2 \right\rangle - \left\langle \sum_n \lambda_n^{N_\tau-1} \text{Re} \left(e^{2\pi ki/3} \langle n | \hat{U}_4 | n \rangle \right) \right\rangle^2}. \quad (2.78)$$

Here, $\langle x \rangle$ denotes an average over all gauge configurations.

These relations (2.74)–(2.77) are satisfied both in full QCD and at the quenched level like the case of the Polyakov loop, namely Eq. (2.17). All these relations are derived on the temporally odd-number lattice for practical reasons. Of course, the relations on the even lattice can be derived by Eq. (2.23), and both choices of the parity for the lattice size in time direction give the same content of physics. However, the continuum limit is hard to practically perform. For example, the renormalization of the Polyakov loop has not been determined. Nevertheless, at least the ambiguity of the multiplicative renormalization of the Polyakov loop can be avoided by

the cancellation of the renormalization function in the ratio of the Polyakov-loop susceptibilities [18, 19].

2.2.3 Numerical Results

In order to numerically investigate the contribution of different Dirac modes to the Polyakov loop susceptibilities and their ratios, we use the above relations. Since the KS formalism can be applicable to the relations, we rewrite the relations using the formula $\langle n | \hat{U}_4 | n \rangle = 4(n | \hat{U}_4 | n)$.

We calculate the contributions from the low-lying Dirac modes to the Polyakov loop fluctuations using the SU(3) lattice QCD Monte Carlo simulations. The numerical setup is the same as the previous section. The Linear Algebra PACKage (LAPACK) [7] is used for diagonalization of the KS Dirac operator to obtain the eigenvalues λ_n and the eigenfunctions $\chi_n(s)$. The lattice spacing a is determined by the string tension $\sigma = 0.89 \text{ GeV/fm}$ on a large lattice at each β at zero temperature. In this setup, in the confinement phase, the average of the plaquette is calculated as $\langle U_{\mu\nu} \rangle = 0.53(2)$. This is consistent with the previous SU(3) lattice studies [20]. In deconfined phase, the average value of plaquette is $\langle U_{\mu\nu} \rangle = 0.60(2)$, which is also consistent with the previous works [20]. For each value of $\beta = 5.6$ and $\beta = 6.0$, we use 20 gauge configurations, which are taken every 500 sweeps after the thermalization of 5000 sweeps.

Like the case of the Polyakov loop itself, the infrared cutoff Λ is introduced and we investigate the influence of the low-lying Dirac modes below Λ . Then, we introduce the Λ -dependent Polyakov loops,

$$|L|_\Lambda = \frac{(2a)^{N_\tau-1}}{3V} \left| \sum_{|\lambda_n| > \Lambda} \lambda_n^{N_\tau-1} (n | \hat{U}_4 | n) \right|, \quad (2.79)$$

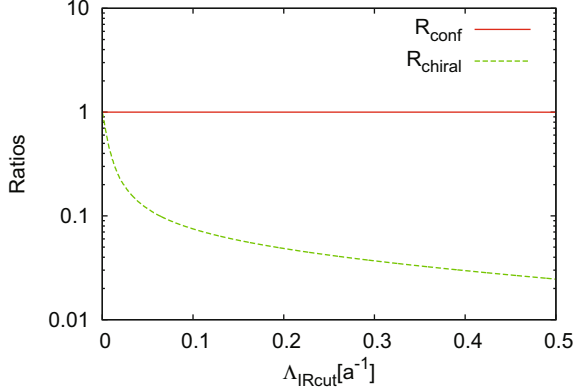
for the modulus, and

$$(L_L)_\Lambda = C_\tau \sum_{|\lambda_n| > \Lambda} \lambda_n^{N_\tau-1} \text{Re} \left(e^{2\pi k i / 3} (n | \hat{U}_4 | n) \right), \quad (2.80)$$

$$(L_T)_\Lambda = C_\tau \sum_{|\lambda_n| > \Lambda} \lambda_n^{N_\tau-1} \text{Im} \left(e^{2\pi k i / 3} (n | \hat{U}_4 | n) \right). \quad (2.81)$$

for the real and the imaginary part, respectively, with $C_\tau = (2ai)^{N_\tau-1}/3V$. Applying the cutoff dependent Polyakov loops from Eqs. (2.79), (2.80) and (2.81) to Eqs. (2.68)–(2.70), we also introduce the Λ -dependent susceptibilities

Fig. 2.9 The numerical results for the ratios R_{chiral} and R_{conf} from Eqs. (2.87) and (2.88), respectively, as a function of an infrared cutoff Λ introduced on Dirac eigenvalues, expressed in the lattice unit. The Monte Carlo calculations have been performed on the $10^3 \times 5$ lattice with $\beta = 5.6$, and for the quark mass of $m = 5$ MeV. This figure is taken from Ref. [9]



$$T^3(\chi_A)_\Lambda = \frac{N_\sigma^3}{N_\tau^3} [\langle |L|_\Lambda^2 \rangle - \langle |L|_\Lambda \rangle^2] \quad (2.82)$$

$$T^3(\chi_L)_\Lambda = \frac{N_\sigma^3}{N_\tau^3} [\langle (L_L)_\Lambda^2 \rangle - \langle (L_L)_\Lambda \rangle^2] \quad (2.83)$$

$$T^3(\chi_T)_\Lambda = \frac{N_\sigma^3}{N_\tau^3} [\langle (L_T)_\Lambda^2 \rangle - \langle (L_T)_\Lambda \rangle^2], \quad (2.84)$$

where, and their ratios

$$(R_A)_\Lambda = \frac{(\chi_A)_\Lambda}{(\chi_L)_\Lambda}, \quad (2.85)$$

$$(R_T)_\Lambda = \frac{(\chi_T)_\Lambda}{(\chi_L)_\Lambda}. \quad (2.86)$$

In order to investigate the influence of the low-lying Dirac modes to the properties of the Polyakov loop fluctuations and the chiral condensate, we introduce two ratios. The cutoff-dependent chiral condensate $\langle \bar{q}q \rangle_\Lambda$ in Eq. (2.63) and the ratio

$$R_{\text{chiral}} = \frac{\langle \bar{q}q \rangle_\Lambda}{\langle \bar{q}q \rangle} \quad (2.87)$$

for chiral symmetry breaking. In the same spirit, we introduce the ratio,

$$R_{\text{conf}} = \frac{(R_A)_\Lambda}{R_A}, \quad (2.88)$$

in order to quantify the sensitivity of the Polyakov loop fluctuations to the particular Dirac modes. When, the ratio satisfies $R_{\text{conf}} \simeq 1$, then the low-lying Dirac modes below the IR cutoff Λ are not essential to the Polyakov loop fluctuations.

Table 2.5 Numerical results for the original values of the Polyakov-loop fluctuations, and IR cut fluctuations with the IR-cutoff $\Lambda \simeq 0.4$ GeV. The results are obtained in quenched QCD on $10^3 \times 5$ lattice with $\beta = 5.6$ (confined phase) and $\beta = 6.0$ (deconfined phase) with 20 gauge configurations. This table is essentially same as that in Ref. [9]

β		Original	IR-cut
$\beta = 5.6$	$T^3 \chi_A$	3.475×10^{-4}	3.470×10^{-4}
	$T^3 \chi_L$	5.307×10^{-4}	5.298×10^{-4}
	$T^3 \chi_T$	6.005×10^{-4}	5.994×10^{-4}
	R_A	0.6548	0.6549
	R_T	1.131	1.131
$\beta = 6.0$	$T^3 \chi_A$	2.965×10^{-3}	2.965×10^{-3}
	$T^3 \chi_L$	3.015×10^{-3}	3.015×10^{-3}
	$T^3 \chi_T$	7.848×10^{-4}	7.848×10^{-4}
	R_A	0.9834	0.9834
	R_T	0.2603	0.2603

The numerical results for the ratios R_{conf} and R_{chiral} in a confined phase at $\beta = 5.6$, for various values of the infrared cutoff Λ in Fig. 2.9. The ratio R_{chiral} is calculated with the quark mass $m = 5$ MeV. From the Fig. 2.9, it is found that the low-lying Dirac modes below Λ have the dominant contribution to the chiral condensate. Thus, the low-lying Dirac modes, which are important modes for chiral symmetry breaking. In contrast to R_{chiral} , the R_{conf} ratio is almost unchanged by the removal of the low-lying Dirac modes even with relatively large cutoff $\Lambda \simeq 0.5$ GeV.

Thus, the important modes for chiral symmetry breaking are not important for confinement properties in QCD. In Table 2.5, the numerical results for the Polyakov loop fluctuations and IR cut fluctuations with the IR-cutoff $\Lambda \simeq 0.4$ GeV. In the deconfinement phase, the same behavior is observed as seen in Table 2.5.

Like the case of the Polyakov loop, we can analytically understand the differences in the influence of the low-lying Dirac modes on the chiral condensate and the Polyakov loop fluctuations. Due to the damping factor $\lambda_n^{N_\tau-1}$, the contributions from the low-lying Dirac modes are strongly suppressed for the Polyakov loops, $|L|$, L_L , L_T from Eqs. (2.75)–(2.77) because the Dirac matrix element $\langle n | \hat{U}_4 | n \rangle$ is finite. Then, since the susceptibilities and their ratios are defined from the Polyakov loops, the low-lying Dirac modes have the negligible contributions to them, too. Thus, the essential modes for chiral symmetry breaking are not essential for a sensitive probe R_A for deconfinement in QCD. This result suggests no direct one-to-one correspondence between confinement and chiral symmetry breaking in QCD. In this way, we have improved the discussion in the previous section by considering the Polyakov loop fluctuations.

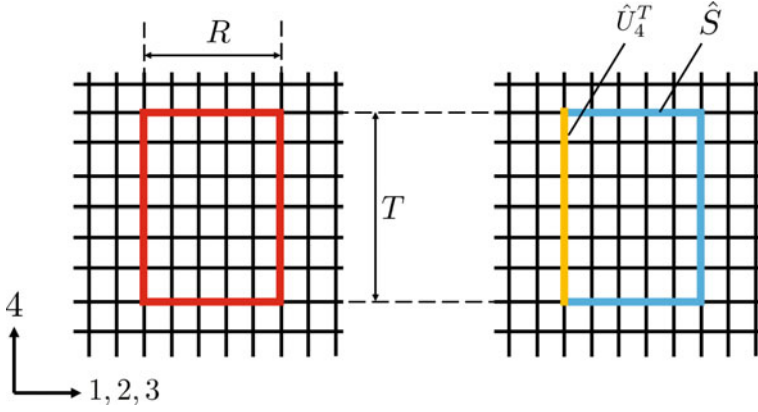


Fig. 2.10 (Left) A rectangular loop with $R \times T$ on the square lattice corresponding to the Wilson loop $W(R, T)$. (Right) The loop is decomposed to the two parts, the staple \hat{S} and the temporal line \hat{U}_{-4}^T

2.3 Wilson Loop

In this section, we derive a formula to express the Wilson loop in terms of the Dirac eigenmodes [3]. In addition to the Polyakov loop and its fluctuations, the Wilson loop is also important quantity for quark-confinement because interquark potential can be defined from the Wilson loop. The formula is valid on an arbitrary square lattice, unlike the formulae for the Polyakov loops. In the following, we show the detailed derivation.

We consider the Wilson loop $W(R, T)$ corresponding to a rectangular loop with $R \times T$, shown in Fig. 2.10. It can be expressed as the functional trace

$$W(R, T) \equiv \text{Tr}_c \left[\hat{U}_1^R \hat{U}_{-4}^T \hat{U}_{-1}^R \hat{U}_4^T \right] = \text{Tr}_c \left[\hat{S} \hat{U}_4^T \right], \quad (2.89)$$

where \hat{S} is the “staple operator” defined as

$$\hat{S} \equiv \hat{U}_1^R \hat{U}_{-4}^T \hat{U}_{-1}^R. \quad (2.90)$$

Like the formula (2.17) for the Polyakov loop, that for the Wilson loop can be derived by introducing a particular functional trace, showing that it is proportional to the Wilson loop, and expanding it with the Dirac eigenmodes. For simplicity, we consider even number T . The functional trace is introduced as

$$J \equiv \text{Tr}_{c,\gamma} \hat{S} \hat{\mathcal{P}}^T, \quad (2.91)$$

where $\hat{\mathcal{P}}$ is given in Eq. (2.3). It corresponds to Eq. (2.14) in Sect. 2.1. We can show that the quantity includes only the Wilson loop. Here, we note that the distance between the end points of the staple operator is T , and the Dirac operator $\hat{\mathcal{P}}$ is expressed as the linear combination of the link-variable operators. Thus, only the \hat{U}_4^T term in the expansion of $\hat{\mathcal{P}}^T$ is only the gauge-invariant term corresponding to the closed loop, namely the Wilson loop.

Therefore, we can obtain

$$\begin{aligned}
 J &= \text{Tr}_{c,\gamma} \hat{S} \hat{\mathcal{P}}^T \\
 &= \text{Tr}_{c,\gamma} \hat{S} (\gamma_4 \hat{D}_4)^T \\
 &= 4 \text{Tr}_c \hat{S} \hat{D}_4^T \\
 &= \frac{4}{(2a)^T} \text{Tr}_c \hat{S} (\hat{U}_4 - \hat{U}_{-4})^T \\
 &= \frac{4}{(2a)^T} \text{Tr}_c \hat{S} \hat{U}_4^T \\
 &= \frac{4}{(2a)^T} W.
 \end{aligned} \tag{2.92}$$

On the other hand, when the Dirac mode is taken as the basis for the functional trace, J is expressed as

$$J = \sum_n \langle n | \hat{S} \hat{\mathcal{P}}^T | n \rangle = (-)^{\frac{T}{2}} \sum_n \lambda_n^T \langle n | \hat{S} | n \rangle, \tag{2.93}$$

where we use the eigenvalue equation (2.4). In this way, we obtain the relation

$$W(R, T) = \frac{(-)^{\frac{T}{2}} (2a)^T}{4} \sum_n \lambda_n^T \langle n | \hat{S} | n \rangle \tag{2.94}$$

for even T . We again note that the low-lying Dirac mode contributions to the Wilson loop is expected to be negligible compared to the other higher modes due to the damping factor λ_n^T . Although the matrix element $\langle n | \hat{S} | n \rangle$ has the explicit T -dependence, the absolute value is finite, and then it does not disturb the argument.

Of course, the similar analysis can be performed in the case of odd number T . In fact, instead of J , when we consider the functional trace for odd T

$$K \equiv \text{Tr}_{c,\gamma} \hat{S} \hat{U}_4 \hat{\mathcal{P}}^{T-1}, \tag{2.95}$$

we can calculate

$$\begin{aligned}
K &= \text{Tr}_{c,\gamma} \hat{S} \hat{U}_4 \hat{D}^{T-1} \\
&= \text{Tr}_{c,\gamma} \hat{S} \hat{U}_4 (\gamma_4 \hat{D}_4)^{T-1} \\
&= \frac{4}{(2a)^{T-1}} \text{Tr}_c \hat{S} \hat{U}_4 (\hat{U}_4 - \hat{U}_{-4})^{T-1} \\
&= \frac{4}{(2a)^{T-1}} \text{Tr}_c \hat{S} \hat{U}_4^T \\
&= \frac{4}{(2a)^{T-1}} W,
\end{aligned} \tag{2.96}$$

and

$$\begin{aligned}
K &= \sum_n \langle n | \hat{S} \hat{U}_4 \hat{D}^{T-1} | n \rangle \\
&= (-)^{\frac{T-1}{2}} \sum_n \lambda_n^{T-1} \langle n | \hat{S} \hat{U}_4 | n \rangle.
\end{aligned} \tag{2.97}$$

Therefore, the similar formula holds for the odd T as

$$W = \frac{(-)^{\frac{T-1}{2}} (2a)^{T-1}}{4} \sum_n \lambda_n^{T-1} \langle n | \hat{S} \hat{U}_4 | n \rangle. \tag{2.98}$$

The indication from Eq. (2.98) is the same as that from Eq. (2.94). That is, the low-lying Dirac modes have little contribution to the Wilson loop.

The $\bar{q}q$ potential $V(R)$ is considered in terms of the Dirac modes using the relation connecting the Wilson loop and the Dirac modes. We consider even T case. In the large T limit, the interquark potential $V(R)$ is extracted as

$$V(R) = - \lim_{T \rightarrow \infty} \frac{1}{T} \ln \langle W(R, T) \rangle. \tag{2.99}$$

Since now the Wilson loop is expressed by the Dirac modes and the relation is valid for arbitrary gauge configuration, the potential $V(R)$ can be expressed as

$$V(R) = - \lim_{T \rightarrow \infty} \frac{1}{T} \ln \left| \left\langle \sum_n (2a \lambda_n)^T \langle n | \hat{S} | n \rangle \right\rangle \right|. \tag{2.100}$$

Similarly, the string tension σ can be expressed as

$$\begin{aligned}
\sigma &= - \lim_{R, T \rightarrow \infty} \frac{1}{RT} \ln \langle W \rangle \\
&= - \lim_{R, T \rightarrow \infty} \frac{1}{RT} \ln \left| \left\langle \sum_n (2a \lambda_n)^T \langle n | \hat{S} | n \rangle \right\rangle \right|.
\end{aligned} \tag{2.101}$$

Again because of the damping factor λ_n^T in the sum, we can find that both the $\bar{q}q$ potential $V(R)$ and the string tension σ are not almost affected by the low-lying Dirac modes unless $\langle n|\hat{S}|n\rangle$ has a counter factor such as λ_n^{-T} . Also for odd T case, similar arguments can be done with Eq. (2.98). Therefore, we directly confirm that the string tension σ , or the confining force, is almost unchanged even if the low-lying Dirac modes disappear, which means chiral symmetry restoration.

References

1. S. Gongyo, T. Iritani, H. Suganuma, Phys. Rev. D **86**, 034510 (2012)
2. T.M. Doi, H. Suganuma, T. Iritani, Phys. Rev. D **90**, 094505 (2014)
3. H. Suganuma, T.M. Doi, T. Iritani, PTEP **2016**, 013B06 (2016)
4. S. Elitzur, Phys. Rev. D **12**, 3978 (1975)
5. J.B. Kogut, L. Susskind, Phys. Rev. D **11**, 395 (1975)
6. H.J. Rothe, *Lattice Gauge Theories* (World Scientific, Singapore, 2012)
7. E. Anderson et al., *LAPACK Users' Guide*, 3rd edn. (Society for Industrial and Applied Mathematics, Philadelphia, 1999)
8. T. Iritani, H. Suganuma, PTEP **2014**, 033B03 (2014)
9. T.M. Doi, K. Redlich, C. Sasaki, H. Suganuma, Phys. Rev. D **92**, 094004 (2015)
10. G. Boyd, J. Engels, F. Karsch, E. Laermann, C. Legeland, M. Lutgemeier, B. Petersson, Phys. Rev. Lett. **75**, 4169 (1995)
11. G. Boyd, J. Engels, F. Karsch, E. Laermann, C. Legeland, M. Lutgemeier, B. Petersson, Nucl. Phys. B **469**, 419 (1996)
12. S. Borsanyi, G. Endrodi, Z. Fodor, S.D. Katz, K.K. Szabo, JHEP **1207**, 056 (2012)
13. F.R. Brown, F.P. Butler, H. Chen, N.H. Christ, Z. Dong, W. Schaffer, Leo I. Unger and Alessandro Vaccarino. Phys. Rev. Lett. **65**, 2491 (1990)
14. R.D. Pisarski, F. Wilczek, Phys. Rev. D **29**, 338 (1984)
15. E. Laermann, O. Philipsen, Ann. Rev. Nucl. Part. Sci. **53**, 163 (2003)
16. A. Bazavov, T. Bhattacharya, M. Cheng, C. DeTar, H.T. Ding, S. Gottlieb, R. Gupta, P. Hegde et al., Phys. Rev. D **85**, 054503 (2012)
17. A. Bazavov et al., HotQCD collaboration. Phys. Rev. D **90**, 094503 (2014)
18. P.M. Lo, B. Friman, O. Kaczmarek, K. Redlich, C. Sasaki, Phys. Rev. D **88**, 014506 (2013)
19. P.M. Lo, B. Friman, O. Kaczmarek, K. Redlich, C. Sasaki, Phys. Rev. D **88**, 074502 (2013)
20. M. Creutz, K.J.M. Moriarty, Phys. Rev. D **26**, 2166 (1982)

Lattice QCD Study for the Relation Between
Confinement and Chiral Symmetry Breaking
Doi, T.

2017, XII, 59 p. 18 illus. in color., Hardcover
ISBN: 978-981-10-6595-8